RSC Advances

This article can be cited before page numbers have been issued, to do this please use: L. Lin and H. Bai, *RSC Adv.*, 2016, DOI: 10.1039/C5RA27488E.

ROYAL SOCIETY OF CHEMISTRY

www.rsc.org/advances

View Article Online
DOI: 10.1039/C5RA27488E

Salt-induced formation of hollow and mesoporous CoO_x/SiO_2 spheres and their catalytic behaviors in toluene oxidation

Liang-Yi Lin[1,2*] and Hsunling Bai[2]

[1]Department of Energy, Environmental and Chemical Engineering, Washington University in St. Louis, St. Louis, MO 63130, United States

[2]Institute of Environmental Engineering, National Chiao Tung University, Hsinchu 300, Taiwan

[*] Corresponding author. E-mail: liangyi1102@gmail.com Tel.: 1-314-637-6523

View Article Online
DOI: 10.1039/C5RA27488E

ABSTRACT

Hollow and mesoporous CoO_x/SiO_2 spheres (denoted as $CoO_x/hSiO_2$ and $CoO_x/mSiO_2$) were synthesized via salt-assisted ultrasonic spray pyrolysis. Precursor solutions containing sodium silicate solution, a mineral acid (hydrochloric acid or nitric acid) and a cobalt salt were ultrasonically aerosolized and pyrolyzed. Results showed that CoO_x/SiO_2 spheres with hollow or mesoporous structure can be fabricated by using the NaCl and $NaNO_3$ salts as in-situ formed templates. Significantly, this approach avoids the need of post calcination for template elimination, instead permitting aqueous removal with water. The influence of the sodium salts on the characteristics of CoO_x/SiO_2 spheres was investigated by means of XRD, nitrogen physisorption, SEM/TEM, ICP-MS, UV-Vis, XPS and H_2-TPR. On the basis of the experimental results, a possible mechanism on the formation of hollow and mesoporous spheres was proposed. The CoO_x/SiO_2 spheres were tested as catalysts for toluene oxidation. The mesoporous $CoO_x/mSiO_2$ was found to exhibit superior activity to hollow $CoO_x/hSiO_2$, probably attributed to a combination of several factors, including predominant existence of Co_3O_4 active phase, high surface Co^{3+} content, and easy reducibility of Co^{3+} at low temperature.

Keywords: ultrasonic spray pyrolysis, hollow, mesoporous, molten salt, cobalt oxide

View Article Online
DOI: 10.1039/C5RA27488E

1. INTRODUCTION

Catalytic oxidation has been proposed as an effective and energy-saving technology for eliminating volatile organic compounds (VOCs) emitted from industrial processes and transport vehicles.[1–3] Recently, cobalt oxide (Co_3O_4) has attracted much attention to control the emissions of VOCs, and it has been considered as a promising alternative to costly noble metal-based catalysts because of its high activity, relatively low price and availability.[4,5] However, the insufficient catalytic performance at low temperatures, narrow operating-temperature window and poor thermal stability of Co_3O_4 largely limit their performance and impede commercialization of VOCs removals.[6–9]

Several studies have been conducted to improve the catalytic activity of cobalt oxide by depositing it on various supports, such as Al_2O_3, ZrO_2, TiO_2, SiO_2 and CeO_2, etc.[10,11] Among available support materials, ordered mesoporous silicas synthesized by surfactant-templating methods have been investigated as promising candidates for catalysis because of their own unique characteristics of high surface area and regular pore structure, which can be used to uniformly disperse the active metal/metal oxide particles.[12–15] Numerous mesoporous silicas, such as MCM-41, SBA-15 and KIT-6 loaded with cobalt oxides for VOCs oxidation have been reported.[16–20] The performance of the supported cobalt oxide catalyst is highly dependent on different synthetic methods as well as precursors.[21,22] Moreover, the crystallinity, oxidation state and surface reducibility of supported cobalt oxide species have been shown to be critical to the activity of the catalyst.[23,24] For preparing highly active catalysts in VOCs oxidation, it is important to obtain Co_3O_4 oxide phase with high surface reducibility.

View Article Online
DOI: 10.1039/C5RA27488E

Although these novel cobalt oxide/mesoporous silica composite catalysts have contributed to recent progress in VOCs removals, they may pose problems in practical field applications because of their high cost. Generally, these composites are synthesized through solution-based batch processes that take several days in a high pressure vessel and require further post-treatments, such as solvent extraction and calcination for template removals.[22,26] Therefore, they are difficult to apply to commercial scale production due to their long processing times, significant batch-to-batch variation and high energy consumption.

Compared to solution-based methods, the aerosol-assisted chemical vapor decomposition, also known as spray pyrolysis, has distinct advantages of rapid synthesis, high product purity, and more importantly, a continuous and scalable process.[27–31] This process involves atomization of a liquid precursor into fine aerosol droplets that are delivered to a heated zone where solvent evaporation and precursor decomposition take place, leading to the deposition of final solid product. The detailed descriptions on this technique can be found in several reviews.[31–33] Recently, Debecker and co-workers[34] synthesized a series of mesoporous WO_3-SiO_2-Al_2O_3 microspheres by the approach combining spray pyrolysis and evaporation induced self-assembly (EISA) of poly(alkylene oxide) block copolymer. Nevertheless, most of the aerosol-based methods reported previously were carried out using expensive silicon precursors (e.g. silicon chloride and silicon alkoxide) and sacrificial templating agents (e.g. surfactant polymers and colloidal polystyrene) as starting precursors,[35] which would increase the manufacturing cost and add pollution to the environment.

View Article Online
DOI: 10.1039/C5RA27488E

In this study, we first report the salt-assisted ultrasonic spray pyrolysis fabrication of cobalt oxide/silica hollow and mesoporous spheres (detonated as $CoO_x/hSiO_2$ and $CoO_x/mSiO_2$) using sodium silicate and cobalt nitrate hydrate as precursors. Compared with traditional aerosol-assisted EISA method for preparing mesoporous silica supported catalysts where costly precursors are employed, the synthesis strategy demonstrated herein is much more inexpensive and energy-saving because no extra templating agents, or high-temperature calcination are required for template removals. The influence of salts on the characteristics of produced spheres is studied in detail by various characterization tools. On the basis of the experimental results, the formation mechanism of hollow and mesoporous spheres is proposed. Further, our experimental results reveal that, compared with pristine Co_3O_4, the $CoO_x/mSiO_2$ demonstrates greatly improved catalytic performance and long-term thermal stability for toluene removal.

2. EXPERIMENTAL SECTION

2.1 Catalyst preparation

Hollow and mesoporous CoO_x/SiO_2 composites were continuously synthesized by a single-step aerosol process in a home-made apparatus depicted in **Scheme 1**. The sodium silicate solution, which is recovered from the silicate waste of liquid crystal display (LCD) manufacturing industry, is used as a low-cost silicon source in this study.[36,37] First, the sodium silicate solution was prepared by mixing LCD industrial waste powder with 6 M NaOH solution at room temperature for 3 h. The elemental composition of raw waste powder and silicate supernatant after extraction with NaOH solution are summarized in

View Article Online
DOI: 10.1039/C5RA27488E

Table S1. Thereafter, a certain amount of HCl or HNO_3 was added to the 189 ml of waste silicate supernatant to bring down the pH value to 2 with constant stirring. Meantime, a calculated amount of cobalt nitrate (dissolved in 20 ml of DI water) was added into the above acidified silicate solution and the combined mixture was stirred for 30 min. The molar composition of the precursor mixture was 1 SiO_2: 2 Na: 0.055 Co: 280 H_2O: 8 HCl, and 1 SiO_2: 2 Na: 0.055 Co: 280 H_2O: 3.7 HNO_3, for $CoO_x/hSiO_2$ and $CoO_x/mSiO_2$, respectively.

The precursor mixture was nebulized by an ultrasonic atomizer (1.8MHz) as carried by high-pressure air (35 psi). The temperature of the heating reactor was controlled at 500 ^oC, and the total synthesis time of this continuous flow process was approximately 5 s to generate the CoO_x/SiO_2 particle. The as-synthesized material was collected downstream of the reactor with a high efficiency filter. Finally, they were recovered by washing and filtration with DI water followed by drying in an oven at 110 ^oC.

To verify the activities of CoO_x/SiO_2 catalysts, the aerosol-made CoO_x/HMSP (hexagonally mesoporous silica particle), which was prepared using commercial silicon precursor via traditional surfactant-templated method, was prepared with similar procedures described in the synthesis of CoO_x/SiO_2 materials. Tetraethoxysilane (TEOS) and cetyltrimethylammonium bromide (CTAB) was selected as the silicon source and mesostructure-directing template, respectively. The molar gel composition of the mixture was 1 SiO_2: 0.18 CTAB: 0.055 Co: 10 ethanol: 80 H_2O: 0.008 HCl. The as-prepared CoO_x/HMSP powder was then placed in a muffle furnace for 6 h at a calcination temperature of 550 ^oC to remove the residual organic template. Detailed description on the synthesized procedure can be referred to Wang and Bai.[38,39] The cobalt loading on the

View Article Online
DOI: 10.1039/C5RA27488E

silica support for all supported catalysts was ca. 5 wt.% according to our experimental results.

The pure Co_3O_4 used in this work was prepared by calcination of $Co(NO_3)_2 \cdot 4H_2O$ at 500 ^oC for 4 h.

2.2 Characterization

The chemical composition of raw waste powder was determined by energy-dispersive X-ray spectroscopy in a scanning electron microscopy (SEM, HITACHI-S4700). The elemental cobalt content in the samples was analyzed by a SCIEX ELAN 5000 inductively coupled plasma-mass spectrometer (ICP-MS). The morphology and structure of the samples were characterized by using SEM (HITACHI-S4700), transmission electron microscopy (TEM, Hitachi H-7100, Japan) and X-ray diffraction (XRD, Rigaku D/MAX-B, Japan, using CuKα radiation *n* source at 1.54A˚). Nitrogen physisorption isotherms of the synthesized materials were measured at -196 ◦C using a surface area and pore diameter distribution analyzer (Micromertitics, ASAP 2020, USA). Pore volumes were obtained from the volumes of nitrogen adsorbed at P/P_o=0.95 or in the vicinity.

The UV-Vis spectra were measured by a spectrophotometer (HITACHI U3010) equipped with a diffuse reflectance integrating sphere coated with aluminum oxide which served as a reference material. All the samples were recorded in the spectral range between 900 and 275 nm. X-ray photoelectron spectroscopy (XPS) measurement was performed on a PHI Quantera with a monochromatic Al Kα source and a charge neutralizer. All the binding energies were calibrated to C 1s peak at 284.8 eV of the surface adventitious carbon. H_2-TPR experiments were performed with an AutoChem II

View Article Online
DOI: 10.1039/C5RA27488E

2920 analyzer. The samples were pre-treated in air at 500 ^{o}C for 2 h. After that, the experiments were carried out from 50 ^{o}C to 900 ^{o}C at a heating rate of 10 ^{o}C/min in 10% H_2/Ar. The H_2 consumption was determined by a thermal conductivity detector (TCD).

2.3 Catalytic removal of gaseous toluene

Catalytic tests were performed by a vertical and downward flow reactor system (i.d. = 0.8 cm). Catalysts were tested in 16-30 mesh (595-1190 μm) powdered form, and a total of 0.1 g catalyst was packed into the middle of the glass reactor supported with thin layers of glass wool on both sides. The reactant feed was composed of 1000 ppm toluene, O_2 and N_2 (balance). The toluene/O_2 molar ratio was 1/200, and the total inlet flow rate was controlled at 100 cm^3/min, which corresponded to a space velocity (SV) of 20,000 h^{-1} at room temperature (25 °C). Prior to each catalytic reaction test, the samples were pretreated under the reaction feed by heating at 120 °C for 2 h, and then cooled to room temperature. Then, reaction temperature was increased stepwise from 100 °C to 500 °C. The catalytic activity was evaluated in terms of toluene conversion. When the complete conversion for toluene oxidation was obtained, the temperature was kept for 33 h to test the reaction stability of the catalyst. To evaluate the reusability of the catalyst, the reuse runs were implemented after the stability test. Each run was kept at 250 °C for 2 h, then the reaction was cooled down to the room temperature. The gas composition after the reaction was analyzed by a gas chromatograph equipped with a flame ionization detector (FID) and a TCD detector.

3. RESULTS AND DISCUSSION

View Article Online
DOI: 10.1039/C5RA27488E

3.1 Catalyst characterization

The wide-angle ($10 \leqq 2\theta \leqq 80°$) powder XRD patterns of as-prepared $CoO_x/hSiO_2$ and as-prepared $CoO_x/mSiO_2$ are depicted in **Fig. 1A**. It can be seen that several diffraction reflections are found in both as-prepared $CoO_x/hSiO_2$ and $CoO_x/mSiO_2$, which can be indexed on crystalline NaCl and $NaNO_3$, respectively. Such an observation can be explained by considering the acidification reaction of sodium silicate by HCl or HNO_3. In the acidification reaction, the silica condensation reactions would occur to form a siloxane linkage between surface silanol groups, which can be represented as:[40]

$$Si(OH)_4 + HO\text{-}Si(OH)_3 \rightarrow (OH)_3Si\text{-}O\text{-}Si(OH)_3 + H_2O \quad (1)$$

And the acidification reaction of sodium silicate solution with HCl and HNO_3, respectively, can be expressed as:

$$Na_2O \cdot xSiO_2 + 2HCl \rightarrow xSiO_2 \downarrow + 2NaCl + H_2O \quad (2)$$

$$Na_2O \cdot xSiO_2 + 2HNO_3 \rightarrow xSiO_2 \downarrow + 2NaNO_3 + H_2O \quad (3)$$

At this time, soluble sodium salts of NaCl or $NaNO_3$ were in-situ formed. During the aerosol process (T= 500 ^oC), the rapid water evaporation would result in the solidification of these sodium salts, which were then embedded in SiO_2 spheres.

For washed CoO_x/SiO_2 samples (**Fig. 1B**), there is a broad reflection at 23^o observed for both two samples, indicating that silica materials are presented in amorphous phase.[41] The lack of visible diffraction reflections due to crystalline NaCl or $NaNO_3$ components reveals that these sodium salts can be easily removed by washing with water. Moreover, it is noticeable that three weak diffraction reflections at $2\theta = 36.9$, 59.4 and 65.2° are found in $CoO_x/mSiO_2$. These diffraction reflections can be assigned to the spinel-structured

View Article Online
DOI: 10.1039/C5RA27488E

Co_3O_4.[22] The presence of visible Co_3O_4 reflections reveals that the Co_3O_4 particles in $CoO_x/mSiO_2$ might be presented in larger particle size or in agglomerated form. On the contrary, both $CoO_x/hSiO_2$ and CoO_x/HMSP show no observable reflections of Co_3O_4. This could be attributed to that the small-sized Co_3O_4 are uniformly distributed and the size of Co_3O_4 particles are below the detection limit of the XRD instrument.[42] The low-angle ($1 \leqq 2\theta \leqq 10°$) powder XRD pattern (**Fig. 1C**) of CoO_x/HMSP shows two well-defined diffraction reflections of (100) and (110) at 2θ of 2.4° and 4.3°, revealing the well-ordered hexagonal mesostructure of CoO_x/HMSP.[39]

The particle morphologies of CoO_x/SiO_2 materials are revealed by SEM and TEM images. As seen in **Fig. 2A** and **2B** that $CoO_x/hSiO_2$ consists of mostly hollow shells or fractured hollow shells (while remaining the spherical shape). In addition, many of these shell structures contain comparatively rough and porous surface. In contrast, as illustrated in **Fig. 2D** and **2E**, spherical particles with well-defined morphologies are observed on $CoO_x/mSiO_2$. It is noteworthy that some well-dispersed tiny particles are locating on the external surface or sitting inside the hollow spheres (**Fig. 2C**). The tiny particles could be assigned to the presence of cobalt oxide particles. And it is found from the HRTEM images (**Fig. 2F**) that the cobalt oxide particles mainly exist between the interconnected pores of $CoO_x/mSiO_2$.

Selected area electron diffraction (SAED) image (**Fig. 2F**, inset) confirms the crystalline nature of the large Co_3O_4 particles ($CoO_x/mSiO_2$ sample). By contrast, no clear diffraction pattern was observed for the $CoO_x/hSiO_2$ sample, suggesting that the cobalt oxides are poorly crystallized. These findings are consistent with the XRD measurements (**Fig. 1A**). The absence of diffraction reflections indicates that the

View Article Online
DOI: 10.1039/C5RA27488E

crystalline domains are very small (at most a few nanometers) and points to polycrystallinity. The $CoO_x/hSiO_2$ and $CoO_x/mSiO_2$ were further characterized through mapping analysis to investigate the Co distribution. As shown in **Fig. S2**, it can be seen that Co species are well-dispersed in both $hSiO_2$ and $mSiO_2$ matrices. On the basis of the above observations, it may conclude that the nature of sodium salt has significant impacts not only on the morphology, but also on the crystallinity of the cobalt oxide particle of CoO_x/SiO_2 composites.

The pore structures of the prepared materials are further analyzed by the nitrogen physisorption measurement, with results displayed in **Fig. 3A**. The $CoO_x/hSiO_2$ exhibits type IV isotherms that possess two-step adsorption isotherm. This type of hysteresis loop has been reported to be associated with hollow particles with nanoporous shell.[43] An adsorption at P/P_o values in the range of 0.3-0.7 could be related to the capillary condensation of nitrogen inside nanopores in the shells, while the second adsorption at P/P_o=0.7-0.9 corresponded to the filling of huge hollow cores, as observed in **Fig. 2A** and **2B**. For $CoO_x/mSiO_2$ sample, a typical single-step type IV isotherms with H2-typed hysteresis loop is observed, which is indicative of mesoporous material having networks of interconnected pores.[44,45] Similarly, CoO_x/HMSP shows a single-step type IV isotherms with clear hysteresis loops at a relative pressure of P/P_o = 0.25−0.45, which is attributed to the presence of intra-particle mesoporosity originated from the surfactant template.[46,47]

The pore size distributions of $CoO_x/hSiO_2$ and $CoO_x/mSiO_2$ calculated by using NLDFT method are shown in **Fig. S1**, and their physico-chemical parameters derived from nitrogen physisorption measurement are summarized in **Table 1**. It is observed that

View Article Online
DOI: 10.1039/C5RA27488E

the formation of multi-modal porous particles are obtained for both $CoO_x/hSiO_2$ and $CoO_x/mSiO_2$. Such phenomenon presumably results from nonuniform solute distribution within the droplet.[48] Compared with CoO_x/SiO_2 samples, the CoO_x/HMSP, which was prepared through surfactant-templating route, clearly exhibits a narrow pore size distribution, suggesting the existence of uniform mesoporosity. And it also exhibits the highest surface area and largest pore volume among all catalysts studied (**Table 1**).

The effect of sodium salts on the physico-chemical properties is also investigated and the results derived from nitrogen physisorption measurement and ICP-MS analyses are summarized in **Table 1**. It is seen that both as-prepared CoO_x/SiO_2 samples show high Na contents, low specific surface area and no porosities. After washing process with water, the surface area and porosities of both samples are significantly increased; meanwhile, the Na content in the as-prepared $CoO_x/hSiO_2$ and $CoO_x/mSiO_2$ samples are reduced to 0.42 and 0.44 wt. %, respectively, in the washed CoO_x/SiO_2 samples. The above results clearly reveal that the NaCl and $NaNO_3$ salts, which are in-situ formed during the acidification process of sodium silicate, can act as effective porogen, which can be then readily removed by washing with water. On the other hand, the cobalt content in the $CoO_x/hSiO_2$ and $CoO_x/mSiO_2$ is 3.09 and 3.95 wt. %, respectively, which is lower than the theoretical content (5 wt. %) in the precursor solution. This is probably due to the incomplete decomposition of cobalt precipitates that would result in some of the cobalt content being carried away during the washing process. Thus, one can conclude that the sodium salts have significant influences not only on the textural properties, but also on the chemical composition of the CoO_x/SiO_2 samples.

The UV-vis spectra of the supported cobalt catalysts are shown in **Fig. 3B**. For

View Article Online
DOI: 10.1039/C5RA27488E

$CoO_x/hSiO_2$ and $CoO_x/mSiO_2$ samples, two absorption bands at 370-390 and around 700 nm are found, which can be related to the Co^{3+} in the octahedral coordination in the Co_3O_4 and to the Co^{2+} in the tetrahedral coordination in the Co_3O_4, indicating the presence of spinel-structured Co_3O_4.[24,49] For CoO_x/HMSP, the wide bands at 525, 585 and 640 nm, typical for tetrahedrally coordinated Co^{2+} due to the metal-ligand charge transfer, are observed. They could be included in amorphous cobalt oxide clusters and Co^{2+}-silicate species.[24] Thus, the spectra indicate the formation of various cobalt oxide species, which are in different interaction with the support.

The XPS analyses were conducted to determine the oxidation state of surface cobalt species, with results shown in **Fig. 3C** and **Table 1**. In the Co XPS spectra, the peaks located at 794.8−797.5 and 779.6-781.2 eV can be ascribed to Co $2p_{1/2}$ and Co $2p_{3/2}$ spin-orbital peaks, respectively.[22] It can be seen the binding energy of Co $2p_{3/2}$ for $CoO_x/mSiO_2$ is 779.6 eV, and the spin-orbit separation between Co $2p_{3/2}$ and Co $2p_{1/2}$, Δ(Co $2p_{3/2}$-$2p_{1/2}$) of $CoO_x/mSiO_2$ is 15.2 eV (**Table 1**). The above results are indicative of the existence of Co^{3+} in Co_3O_4.[22] For $CoO_x/hSiO_2$ and CoO_x/HMSP samples, the binding energies of Co $2p_{3/2}$ are increased to 780.9 and 781.2 eV, respectively, accompanying with intense satellite peaks at ca. 785.5 eV, which have been reported as the evidence of the progressive formation of Co^{2+} species. Meanwhile, the Δ(Co $2p_{3/2}$-$2p_{1/2}$) of $CoO_x/hSiO_2$ and CoO_x/HMSP increase to 15.8 and 16.3, respectively, demonstrating the decrease in the surface Co^{3+} content.[22,50] Besides, the relative surface contents of Co^{3+} (Co^{3+}/ (Co^{3+}+ Co^{2+})), which was calculated from peak I/peal II area in **Fig. 3C**, decreases in the order of $CoO_x/mSiO_2$ > $CoO_x/hSiO_2$ > CoO_x/HMSP. Accordingly, one can conclude that the synthetic procedure greatly influences the oxidation state of surface

View Article Online
DOI: 10.1039/C5RA27488E

cobalt species. The surface Co^{3+} content is the highest on $CoO_x/mSiO_2$, while CoO_x/HMSP exhibits the lowest content of surface Co^{3+}.

The surface reducibility of the catalysts studied by the H_2-TPR measurement are displayed in **Fig. 3D**. For $CoO_x/mSiO_2$ sample, four main reduction peaks centering at 279, 482, 720 and 771 ^oC can be clearly observed. By analogy with previous studies, the first peak is indicative for the reduction of Co^{3+} to Co^{2+}, while the second peak is associated with the reduction of CoO to metallic Co.[20,21,50] The broad peak between 600 to 900 ^oC is attributed to the reduction of the remaining Co^{2+} and highly dispersed tetrahedral coordinated Co^{2+}-silicate-like species with strong interaction with the support.[51,52] Compared with $CoO_x/mSiO_2$, $CoO_x/hSiO_2$ sample displays a progressive shift of the H_2 consumption peak to higher temperatures, indicating decreased reducibility. The TPR profile of CoO_x/HMSP differs significantly from those of other samples. Three weak reduction peaks can be found at 262, 380, and 535 ^oC, respectively, which could be ascribed to the reduction of Co^{3+} and CoO to metallic Co. Additionally, a sharp reduction peak at 730 ^oC with a shoulder at 806 ^oC are also observed. They might be mainly originated from the reduction of Co^{2+} and Co^{2+}-silicate-like species, and the above observation is in good agreement with UV-Vis and XPS results. It has been reported that the nature of the support affects the particle size, and the low-surface-area supports promote the agglomeration of cobalt particles as larger Co_3O_4 crystals, which are easily reduced in comparison with smaller particles.[23,49] According to this, the high-surface-area HMSP support may provide a suitable environment for the formation of small-sized and highly dispersed cobalt oxide species, which interact strongly with the support, and thus had a detrimental effect on the surface reducibility.

View Article Online
DOI: 10.1039/C5RA27488E

It has been reported that reduction of Co^{3+} species is one of the crucial factors that determines the activity of cobalt oxide catalyst.[22,53] Wu et al.[21] showed that Co_3O_4-CeO_2 mixed oxides with a lower reduction temperature of Co^{3+} presented higher catalytic activity in methane oxidation. It is clear that high surface reducibility favors high catalytic activity since the reduction of reactive surface species frequently occurs at relatively lower temperature. In this study, for the reduction of Co^{3+} in the TPR profiles, CoO_x/mSiO_2 has a relatively lower reduction temperature (279 ^oC) and the highest H_2 consumption of Co^{3+} amount among all supported catalysts. This indicates that CoO_x/mSiO_2 has the highest amount of easily reducible Co^{3+}. On the other hand, in spite of the lowest reduction temperature of Co^{3+} (262 ^oC), CoO_x/HMSP shows the lowest H_2 consumption amount of Co^{3+}, suggesting that it contains the least amount of easily reducible Co^{3+} species.

3.2 Formation mechanism

It is of particular interest to understand the formation mechanism of CoO_x/hSiO_2 and CoO_x/mSiO_2 particles considering that the hollow shell and mesoporous morphologies are obtained without the use of extra templates. On the basis of the aforementioned results, a possible formation pathway of CoO_x/hSiO_2 and CoO_x/mSiO_2 particles is proposed in **Scheme 2**. At first, precursor sols were firstly prepared via the acidification of LCD waste-derived sodium silicate solution by adding either HCl or HNO_3; meanwhile, the soluble sodium salts of NaCl or $NaNO_3$ were in-situ formed. Subsequently, cobalt nitrate was added as a metal precursor.

As the precursor was aerosolized and entered a heated zone (500 ^oC), the rapid

View Article Online
DOI: 10.1039/C5RA27488E

water evaporation resulted in a temperature gradient within the aerosol droplet, with the surface of the aerosol droplets being heated first and then heat being transferred to the core. Secondly, when heating of the droplet proceeded, water containing dissolved salts like NaCl diffused from the interface to the core due to the improved ion concentration at the interface because of water evaporation; simultaneously, the silica and cobalt species would cross-link with each other and form cobalt-silicate species by isolating the structural hydroxyl neighbors during the thermal treatment at 500 ^{o}C. The cobalt-silicate aggregate acted as a shell, and salts began to nucleate and be fixed by primary units. Thirdly, when water evaporated completely, NaCl crystallized and aggregated as a core, while the thermal decomposition of the precursor of cobalt-silicate might yield cobalt hydroxide, which was subsequently transformed to CoO/Co_3O_4. Finally, $CoO_x/hSiO_2$ hollow particles were produced after the removal of NaCl by washing with water.

In contrast to $CoO_x/hSiO_2$, $CoO_x/mSiO_2$ particle with well-defined morphology and mesoporous structure is observed. Similarly, the $NaNO_3$ diffused from the interface to the core due to rapid water evaporation during aerosol process. As the process continued, the $NaNO_3$ (melting point = 308 ^{o}C) would become molten and served as a solvent, diffusing back into the interface in response to the concentration gradient. After washing with water, $CoO_x/mSiO_2$ having interconnected mesopores were obtained.

Moreover, unlike NaCl, which is thermally stable up to 800 ^{o}C, $NaNO_3$ might be being thermally decomposed in the present case. This was further confirmed by the TG/DTG analyses. As seen in **Fig. S3A**, both as-prepared $CoO_x/hSiO_2$ and $CoO_x/mSiO_2$ samples showed initial weight losses from 100 to 300 ^{o}C, which can be ascribed to the evaporation of moisture on the catalyst surface, and the decomposition of cobalt

View Article Online
DOI: 10.1039/C5RA27488E

precursor.[54] Interestingly, it is noted that there is a drastic weight loss from 300 to 800 ^{o}C on as-prepared CoO_x/mSiO_2 (**Fig. S3A** and **3B**), which can be attributed to the thermal decomposition of $NaNO_3$.[55] In spite of the rapid heating rates experienced by the droplet in aerosol process, the residence time of the droplet in the heated zone (5 s) was too short for complete decomposition of $NaNO_3$. And this was verified by the XRD analysis (**Fig. 1A**), where diffraction reflections of crystalline $NaNO_3$ were clearly observed. Consequently, one may deduce that only a certain amount of $NaNO_3$ was being thermally decomposed in aerosol process.

The decomposition products from $NaNO_3$, such as O_2, may further catalyze the oxidation of Co^{2+} yielding Co^{3+}, accompanying the formation of spinel-structured Co_3O_4. Although oxidizing gases may be produced from the inherent decomposition of cobalt nitrate, the predominant existence of Co^{2+} species on both CoO_x/hSiO_2 and CoO_x/HMSP samples, as revealed by XPS studies, suggests that the impact of these low concentration gases on the nature of supported cobalt species is negligible. The above results clearly demonstrate that the NaCl and $NaNO_3$ salts, which were in-situ formed during the acidification process of sodium silicate, played crucial roles on affecting the pore structure, oxidation state and surface reducibility of CoO_x/SiO_2 materials.

3.3 Toluene oxidation over various catalysts

In the blank experiment (without any catalyst), no conversion of toluene was detected below 500 ^{o}C under the conditions of toluene concentration= 1000 ppm and the GHSV= 20,000 h^{-1}, revealing that the direct thermal incineration of toluene

View Article Online
DOI: 10.1039/C5RA27488E

was negligible under the adopted conditions. **Fig. 4A** displays the toluene conversion as a function of temperature over $CoO_x/hSiO_2$, $CoO_x/mSiO_2$, CoO_x/HMSP and Co_3O_4 catalysts. Obviously, the toluene conversion increased with the rise in reaction temperature and toluene was completely oxidized over all catalysts below 500 ^oC. The final products in the reaction were only CO_2 and H_2O, and no other by-products were detected.

The activities of the catalysts are evaluated by T_{50} and T_{90}, corresponding to the temperature at 50% and 90% of toluene conversion, and decrease in the order of $CoO_x/mSiO_2$ (185 and 230 ^oC) > Co_3O_4 (230 and 245 ^oC) > $CoO_x/hSiO_2$ (260 and 290 ^oC) > CoO_x/HMSP (400 and 430 ^oC). For VOCs oxidation over supported cobalt catalysts, it is well-known that the catalytic performance is associated with a number of parameters of catalyst, such as the crystallinity of supported cobalt oxide, nature of the support, and reducibility of the cobalt species.[21,22,56] The support material having high surface area and large pore volume is reported to be favorable for dispersing active particles and improving the efficiency of the catalyst.[57,58] In this work, however, it is worth pointing out that the catalytic activity of CoO_x/HMSP is much inferior to those of $CoO_x/hSiO_2$ and $CoO_x/mSiO_2$, even though it consists of well-ordered mesostructure, and much higher surface area and pore volume (872 m^2/g, 0.61 cm^3/g) than those of $CoO_x/hSiO_2$ and $CoO_x/mSiO_2$ samples (411 m^2/g, 0.34 cm^3/g; 471 m^2/g, 0.47 cm^3/g). In this sense, $S_{BET,}$ V_{pore} and pore structure are minor factors for affecting the toluene oxidation in these supported cobalt catalysts.

View Article Online
DOI: 10.1039/C5RA27488E

The metal content is one of the crucial parameters that affect the activity of the supported catalyst. As shown in **Table 1**, the cobalt contents of the samples decrease in the order of CoO_x/HMSP > CoO_x/$mSiO_2$ > CoO_x/$hSiO_2$. However, the order of the cobalt content is not fully in line with the results of catalytic tests. It is therefore deduced that the cobalt content is not the key factor determining the activity of these catalysts. Alternatively, the UV-vis spectra, XPS and H_2-TPR analyses suggest that the amount of spinel-structured Co_3O_4 with respect to Co^{3+} species decreases in the order of CoO_x/$mSiO_2$ > CoO_x/$hSiO_2$ > CoO_x/HMSP, which is perfectly consistent with the order of catalytic tests. According to the literature, it is known that the predominant formation of Co_3O_4 oxide phase with facile reducibility of Co^{3+} species on the support is advantageous for efficient VOCs oxidation,[16,17,24] which can well elucidate the highest catalytic activity of CoO_x/$mSiO_2$ catalyst. For CoO_x/$hSiO_2$ sample, its open-hollow structure with nanoporous shell might allow the toluene molecules access to the active cobalt sites more easily; however, its relatively weaker surface reducibility resulted in a higher reaction temperature.

On the opposite, the poorest performance of CoO_x/HMSP should be related to its highest amount of hardly reducible Co^{2+} and Co^{2+}-silicate-like species, which are considered inactive in the studied reaction. Considering the results of structure-performance relationship, one can conclude that the presence of Co_3O_4 oxide phase with high amount of easily reducible Co^{3+} species is favorable for high catalytic activity on toluene oxidation. Besides, it is also found that the catalytic activity over CoO_x/$mSiO_2$ is higher than unsupported Co_3O_4 catalyst. Thus it is reasonable

View Article Online
DOI: 10.1039/C5RA27488E

to suggest that $mSiO_2$ support shows a significant promoting effect for the activity of cobalt oxide catalysts, and this could be related with the higher dispersion and enhanced reducibility of cobalt oxide species on $mSiO_2$.[59,60]

3.4 Stability of $CoO_x/mSiO_2$ catalyst

Fig. 4B depicts the time-dependent catalytic performance of $CoO_x/mSiO_2$ under conditions of 1000 ppm toluene at a temperature of T_{100} (250 ^oC). Since unsupported Co_3O_4 showed almost complete removal of toluene at 250 ^oC (**Fig. 4A**), its durability was also investigated for comparison. Initially, the conversion of toluene over unsupported Co_3O_4 slightly decreased from 98.6% to 95.1% and can be well sustained during the following 16 h. Then it quickly decreased to 62% within 2 h and then completely deactivated after running for 29 h on stream. Conversely, the toluene conversion over $CoO_x/mSiO_2$ catalyst almost kept constant at 94% after running for 33 h, revealing its excellent tolerance and catalytic stability. **Fig. 4C** shows the reuse performance of $CoO_x/mSiO_2$ during 5 cycles of operation. It can be seen that the toluene conversion was very stable and exhibited within 1% attrition during the 5 cycles of operation. On the basis of the obtained results, one can conclude that the synthesized $CoO_x/mSiO_2$ possessed good stability and durability.

The XRD and nitrogen physisorption analyses of the used Co_3O_4 and $CoO_x/mSiO_2$ samples were tested and shown in **Fig. S4** and **Table S2**. The XRD patterns show that the crystallinity of used Co_3O_4 sample diminishes considerably as compared with that of fresh one. It is known that water is produced during VOCs oxidation and always has a negative effect on the catalyst structure.[61,62] In this work, the deactivation of unsupported

View Article Online
DOI: 10.1039/C5RA27488E

Co_3O_4 catalyst could be associated with the collapse of active Co_3O_4 component by the presence of moisture. Conversely, there is no significant difference observed in the XRD and surface area results between fresh and used $CoO_x/mSiO_2$ samples. Moreover, the Co 2p region XPS spectra (**Fig. S5**) also reveal that after the catalytic test in toluene oxidation, the signal intensities of used $CoO_x/mSiO_2$ only weakened slightly with respect to fresh sample, and the binding energies were nearly unchanged, indicating that active cobalt oxides can be well-stabilized and effectively preserved on $mSiO_2$ support during consecutive reaction. This high stability of the active cobalt oxide particles together with the mesostructure preservation are the key factors for the excellent activity of $CoO_x/mSiO_2$ catalyst.

4. Conclusions

By adopting a rapid and single-step salt-assisted aerosol method, hollow and mesoporous CoO_x/SiO_2 spheres were synthesized without using extra pore templates. The XRD, nitrogen physisorption, ICP-MS, UV-Vis, XPS, and H_2-TPR results clearly showed that the sodium salts, which were in-situ formed during the acidification of sodium silicate solution, had significant impacts on the crystallinity, cobalt content, textural structure, oxidation state and surface reducibility of CoO_x/SiO_2 catalysts. The catalytic behaviors of CoO_x/SiO_2 catalysts were further investigated in catalytic oxidation of toluene at temperature range of 100-500 ^oC. It was demonstrated that mesoporous $CoO_x/mSiO_2$ performed better than the hollow $CoO_x/hSiO_2$, probably due to a combination of several factors of predominant existence of Co_3O_4 active phase, high surface Co^{3+} content, and easy reducibility of Co^{3+} at low temperature. This facile method

View Article Online
DOI: 10.1039/C5RA27488E

could be extendable to the preparation of various hollow and mesoporous silica supported composites for a wide range of environmental applications.

Acknowledgment

The authors gratefully acknowledge the financial support from the Ministry of Science and Technology of Taiwan, R.O.C. through grant No.: NSC 102-2221-E-009-009-MY3.

References

1 H. Huang, Y. Xu, Q. Feng and D. Y. C. Leung, *Catal. Sci. Technol.*, 2015, **5**, 2649–2669.

2 J. W. Li, K. L. Pan, S. J. Yu, S. Y. Yan and M. B. Chang, *J. Environ. Sci.*, 2014, **26**, 2546–2553.

3 H. C. Wang, H. S. Liang and M. B. Chang, *J. Hazard. Mater.*, 2011, **186**, 1781–1787.

4 L. F. Liotta, H. Wu, G. Pantaleo and A. M. Venezia, *Catal. Sci. Technol.*, 2013.

5 T. Garcia, S. Agouram, J. F. Sánchez-Royo, R. Murillo, A. M. Mastral, A. Aranda, I. Vázquez, A. Dejoz and B. Solsona, *Appl. Catal. Gen.*, 2010, **386**, 16–27.

6 M. F. M. Zwinkels, S. G. Järås, P. G. Menon and T. A. Griffin, *Catal. Rev.*, 1993, **35**, 319–358.

7 A. Y. Khodakov, J. Lynch, D. Bazin, B. Rebours, N. Zanier, B. Moisson and P. Chaumette, *J. Catal.*, 1997, **168**, 16–25.

8 L. F. Liotta, G. Di Carlo, G. Pantaleo, A. M. Venezia and G. Deganello, *Appl. Catal. B Environ.*, 2006, **66**, 217–227.

View Article Online
DOI: 10.1039/C5RA27488E

9 D. L. Trimm, *Catal. Today*, 1995, **26**, 231–238.

10 Z. Zhao, M. M. Yung and U. S. Ozkan, *Catal. Commun.*, 2008, **9**, 1465–1471.

11 M. M. Yung, Z. Zhao, M. P. Woods and U. S. Ozkan, *J. Mol. Catal. Chem.*, 2008, **279**, 1–9.

12 S.-H. Wu, C.-Y. Mou and H.-P. Lin, *Chem. Soc. Rev.*, 2013, **42**, 3862–3875.

13 C.-C. Li, U.-T. Wu and H.-P. Lin, *J. Mater. Chem. A*, 2014, **2**, 8252–8257.

14 C.-C. Li, Y.-W. Chen, R.-J. Lin, C.-C. Chang, K.-H. Chen, H.-P. Lin and L.-C. Chen, *Chem. Commun.*, 2011, **47**, 9414–9416.

15 C.-K. Chen, Y.-W. Chen, C.-H. Lin, H.-P. Lin and C.-F. Lee, *Chem. Commun.*, 2009, **46**, 282–284.

16 Á. Szegedi, M. Popova and C. Minchev, *J. Mater. Sci.*, 2009, **44**, 6710–6716.

17 Z. Mu, J. J. Li, M. H. Duan, Z. P. Hao and S. Z. Qiao, *Catal. Commun.*, 2008, **9**, 1874–1877.

18 S. Zuo, F. Liu, J. Tong and C. Qi, *Appl. Catal. Gen.*, 2013, **467**, 1–6.

19 Z. Mu, J. J. Li, H. Tian, Z. P. Hao and S. Z. Qiao, *Mater. Res. Bull.*, 2008, **43**, 2599–2606.

20 T. Tsoncheva, L. Ivanova, J. Rosenholm and M. Linden, *Appl. Catal. B Environ.*, 2009, **89**, 365–374.

21 H. Wu, G. Pantaleo, G. D. Carlo, S. Guo, G. Marcì, P. Concepción, A. M. Venezia and L. F. Liotta, *Catal. Sci. Technol.*, 2015, **5**, 1888–1901.

22 Z. Zhu, G. Lu, Z. Zhang, Y. Guo, Y. Guo and Y. Wang, *ACS Catal.*, 2013, **3**, 1154–1164.

23 J.-S. Girardon, E. Quinet, A. Griboval-Constant, P. A. Chernavskii, L. Gengembre and A. Y. Khodakov, *J. Catal.*, 2007, **248**, 143–157.

View Article Online
DOI: 10.1039/C5RA27488E

24 M. Popova, A. Ristić, V. Mavrodinova, D. Maučec, L. Mindizova and N. N. Tušar, *Catal. Lett.*, 2014, **144**, 1096–1100.

25 Z. ZHANG, Y. LIANG, Q. REN, H. LIU and Y. CHEN, *Chin. J. Catal.*, 2011, **32**, 250–257.

26 W.-N. Wang, J. Park and P. Biswas, *Catal. Sci. Technol.*, 2011, **1**, 593–600.

27 L. Liu, C. Zhao, H. Zhao, D. Pitts and Y. Li, *Chem. Commun.*, 2013, **49**, 3664–3666.

28 S. H. Choi, Y. J. Hong and Y. C. Kang, *Nanoscale*, 2013, **5**, 7867–7871.

29 Y. J. Hong and Y. C. Kang, *Nanoscale*, 2014, **7**, 701–707.

30 C. Zhao, L. Liu, H. Zhao, A. Krall, Z. Wen, J. Chen, P. Hurley, J. Jiang and Y. Li, *Nanoscale*, 2013, **6**, 882–888.

31 N. E. Motl, A. K. P. Mann and S. E. Skrabalak, *J. Mater. Chem. A*, 2013, **1**, 5193–5202.

32 C. Boissiere, D. Grosso, A. Chaumonnot, L. Nicole and C. Sanchez, *Adv. Mater.*, 2011, **23**, 599–623.

33 J. H. Bang and K. S. Suslick, *Adv. Mater.*, 2010, **22**, 1039–1059.

34 D. P. Debecker, M. Stoyanova, U. Rodemerck, F. Colbeau-Justin, C. Boissère, A. Chaumonnot, A. Bonduelle and C. Sanchez, *Appl. Catal. Gen.*, 2014, **470**, 458–466.

35 C. Gérardin, J. Reboul, M. Bonne and B. Lebeau, *Chem. Soc. Rev.*, 2013, **42**, 4217–4255.

36 L.-Y. Lin, J.-T. Kuo and H. Bai, *J. Hazard. Mater.*, 2011, **192**, 255–262.

37 L.-Y. Lin and H. Bai, *Environ. Sci. Technol.*, 2013, **47**, 4636–4643.

38 C. Y. Wang and H. Bai, *Catal. Today*, 2011, **174**, 70–78.

39 C. Wang and H. Bai, *Ind. Eng. Chem. Res.*, 2011, **50**, 3842–3848.

40 J. Schlomach and M. Kind, *J. Colloid Interface Sci.*, 2004, **277**, 316–326.

View Article Online
DOI: 10.1039/C5RA27488E

41 H. Isobe, S. Utsumi, K. Yamamoto, H. Kanoh and K. Kaneko, *Langmuir*, 2005, **21**, 8042–8047.

42 A. Prabhu, L. Kumaresan, M. Palanichamy and V. Murugesan, *Appl. Catal. Gen.*, 2010, **374**, 11–17.

43 C. Y. Jung, J. S. Kim, T. S. Chang, S. T. Kim, H. J. Lim and S. M. Koo, *Langmuir*, 2010, **26**, 5456–5461.

44 M. Karthik, A. Faik, S. Doppiu, V. Roddatis and B. D'Aguanno, *Carbon*, 2015, **87**, 434–443.

45 M. Karthik, E. Redondo, E. Goikolea, V. Roddatis, S. Doppiu and R. Mysyk, *J. Phys. Chem. C*, 2014, **118**, 27715–27720.

46 M. Karthik and H. Bai, *Appl. Catal. B Environ.*, 2014, **144**, 809–815.

47 T. Tsoncheva, G. Issa, T. Blasco, M. Dimitrov, M. Popova, S. Hernández, D. Kovacheva, G. Atanasova and J. M. L. Nieto, *Appl. Catal. Gen.*, 2013, **453**, 1–12.

48 S. H. Kim, B. Y. H. Liu and M. R. Zachariah, *Chem. Mater.*, 2002, **14**, 2889–2899.

49 B. Solsona, T. E. Davies, T. Garcia, I. Vázquez, A. Dejoz and S. H. Taylor, *Appl. Catal. B Environ.*, 2008, **84**, 176–184.

50 Q. Wang, Y. Peng, J. Fu, G. Z. Kyzas, S. M. R. Billah and S. An, *Appl. Catal. B Environ.*, 2015, **168–169**, 42–50.

51 Q. Tang, Q. Zhang, P. Wang, Y. Wang and H. Wan, *Chem. Mater.*, 2004, **16**, 1967–1976.

52 C. Wang, S. Lim, G. Du, C. Z. Loebicki, N. Li, S. Derrouiche and G. L. Haller, *J. Phys. Chem. C*, 2009, **113**, 14863–14871.

53 X. Xie, Y. Li, Z.-Q. Liu, M. Haruta and W. Shen, *Nature*, 2009, **458**, 746–749.

54 M. T. Makhlouf, B. M. Abu-Zied and T. H. Mansoure, *Met. Mater. Int.*, 2013, **19**, 489–

View Article Online
DOI: 10.1039/C5RA27488E

495.

55 J. H. Peredes, H. E. Ponce, M. P. Beltran, M. E. Alvarez Ramos and A. D. Moller, *Microsc. Microanal.*, 2007, **13**, 740–741.

56 G. Bai, H. Dai, J. Deng, Y. Liu, F. Wang, Z. Zhao, W. Qiu and C. T. Au, *Appl. Catal. Gen.*, 2013, **450**, 42–49.

57 C. He, X. Zhang, S. Gao, J. Chen and Z. Hao, *J. Ind. Eng. Chem.*, 2012, **18**, 1598–1605.

58 C. He, Q. Li, P. Li, Y. Wang, X. Zhang, J. Cheng and Z. Hao, *Chem. Eng. J.*, 2010, **162**, 901–909.

59 J. Deng, L. Zhang, H. Dai and C.-T. Au, *Appl. Catal. Gen.*, 2009, **352**, 43–49.

60 Z. Qu, Y. Bu, Y. Qin, Y. Wang and Q. Fu, *Appl. Catal. B Environ.*, 2013, **132–133**, 353–362.

61 D. R. Merrill and C. C. Scalione, *J. Am. Chem. Soc.*, 1921, **43**, 1982–2002.

62 C. Hu, Q. Zhu, Z. Jiang, L. Chen and R. Wu, *Chem. Eng. J.*, 2009, **152**, 583–590.

Table 1

Physicochemical parameters of cobalt-based samples.

Sample name	S_{BET} (m^2/g)	V_{Pore} (cm^3/g)	Na content (wt. %)	Cobalt content (wt. %)	Binding energy (eV) $\Delta(Co\ 2p_{3/2}\text{-}2p_{1/2})$
As-prepared $CoO_x/hSiO_2$	13	0.04	7.35	-	-
As-prepared $CoO_x/mSiO_2$	20	0.08	7.48	-	-
Washed $CoO_x/hSiO_2$	411	0.34	0.42	3.09	15.8 (796.7-780.9)
Washed $CoO_x/mSiO_2$	471	0.47	0.44	3.95	15.2 (794.8-779.6)
Calcined CoO_x/HMSP	872	0.61	-	4.88	16.3 (797.5-781.2)
Co_3O_4	13	0.03	-	-	-

View Article Online
DOI: 10.1039/C5RA27488E

Figure Caption

Scheme 1. Schematic drawing illustration the aerosol route and the washing process of $CoO_x/hSiO_2$ and $CoO_x/mSiO_2$ particles.

Fig. 1. (A) Wide-angle XRD patterns of as-prepared $CoO_x/hSiO_2$ and as-prepared $CoO_x/mSiO_2$; **(B)** Wide-angle and **(C)** low-angle XRD patterns of washed $CoO_x/hSiO_2$, washed $CoO_x/mSiO_2$, CoO_x/HMSP and Co_3O_4.

Fig. 2. SEM, TEM and selected area electron diffraction images of $CoO_x/hSiO_2$ (A, B and C) and $CoO_x/mSiO_2$ (D, E and F).

Fig. 3. (A) Nitrogen physisorption isotherm, **(B)** UV-Vis spectra, **(C)** XPS spectra and **(D)** H_2-TPR profiles of $CoO_x/hSiO_2$, $CoO_x/mSiO_2$, and CoO_x/HMSP.

Scheme 2. Scheme representation showing the formation mechanism of $CoO_x/hSiO_2$ and $CoO_x/mSiO_2$ through salt-assisted aerosol process.

Fig. 4. (A) Toluene conversion over (a) $CoO_x/hSiO_2$, (b) $CoO_x/mSiO_2$, (c) CoO_x/HMSP, and (d) Co_3O_4 **(B)** Time-on-stream stability of toluene removal over $CoO_x/mSiO_2$ and Co_3O_4 catalysts at operation temperature of 250 °C. **(C)** Recycling tests for toluene removal over $CoO_x/mSiO_2$ at operation temperature of 250 °C. (Reaction condition: toluene concentration: 1000 ppm, toluene/O_2 molar ratio was 1/200 and SV: 20,000 h^{-1}).

View Article Online
DOI: 10.1039/C5RA27488E

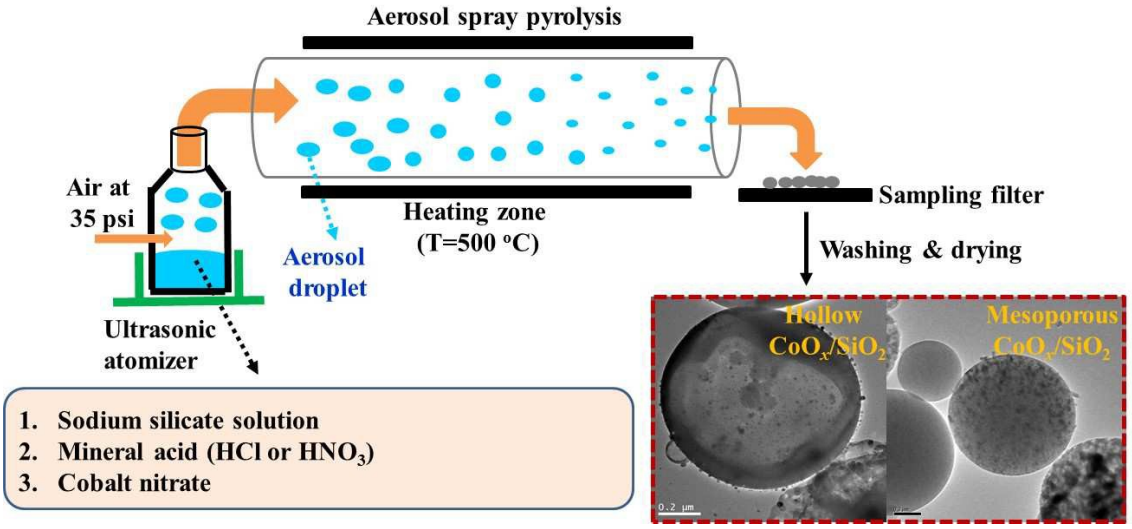

Scheme 1 Schematic drawing illustration the aerosol route and the washing process of $CoO_x/hSiO_2$ and $CoO_x/mSiO_2$ particles.

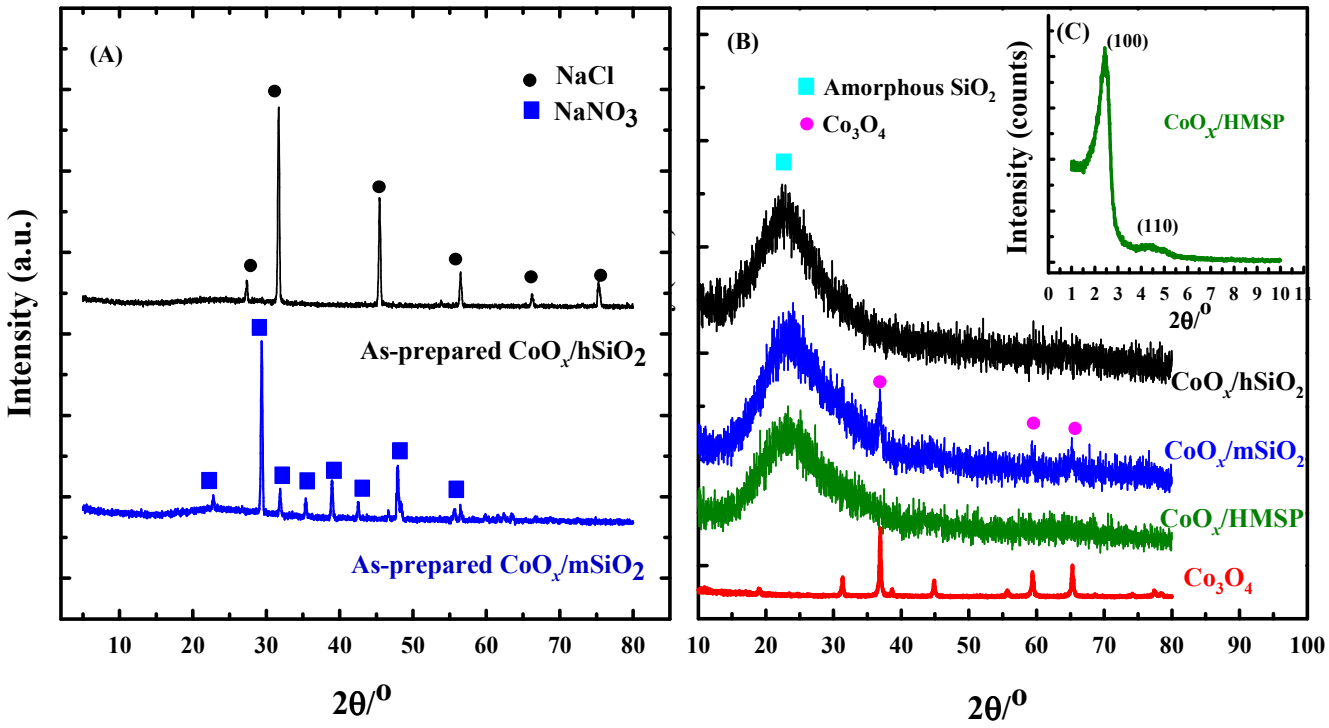

Fig. 1

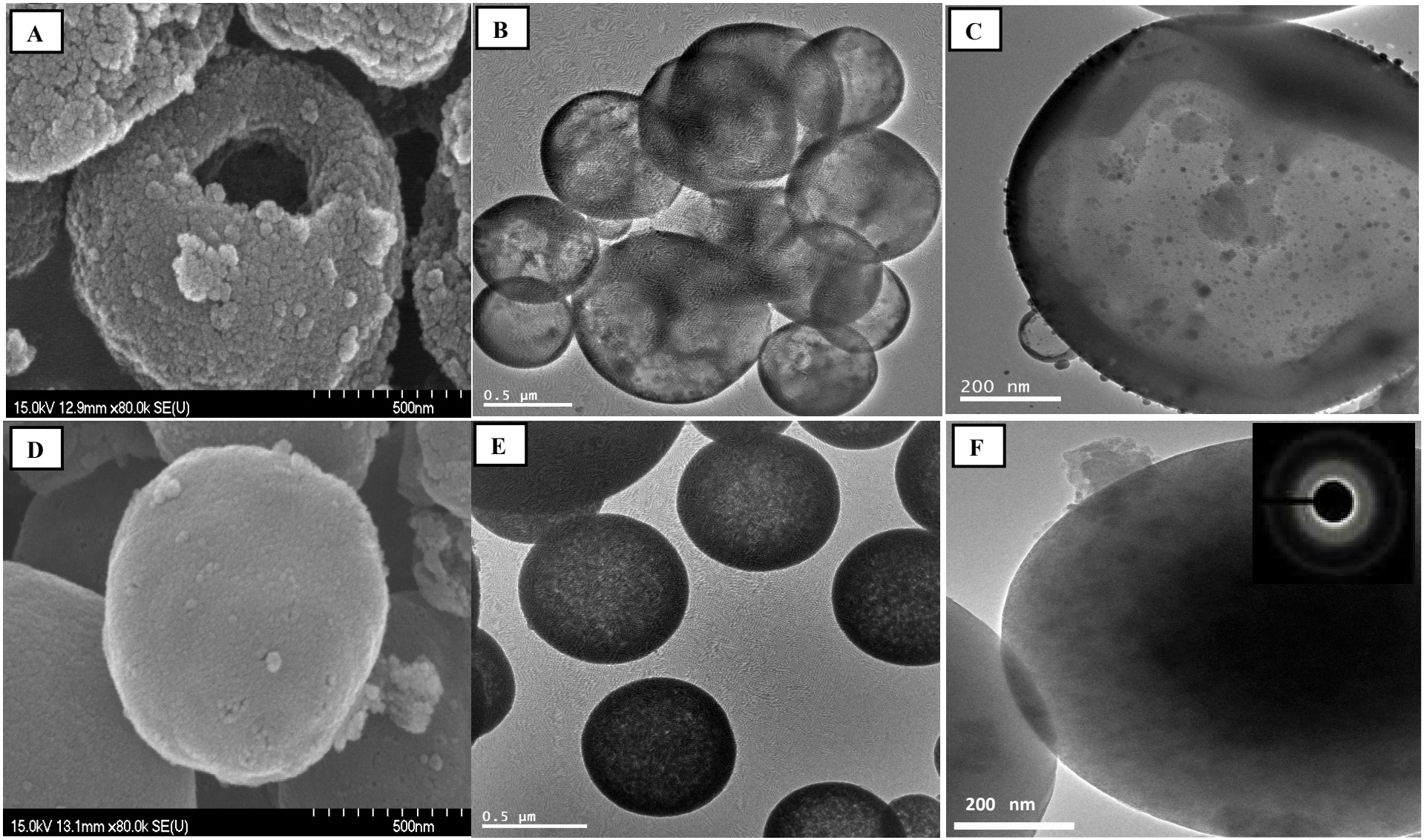

Fig. 2

View Article Online
DOI: 10.1039/C5RA27488E

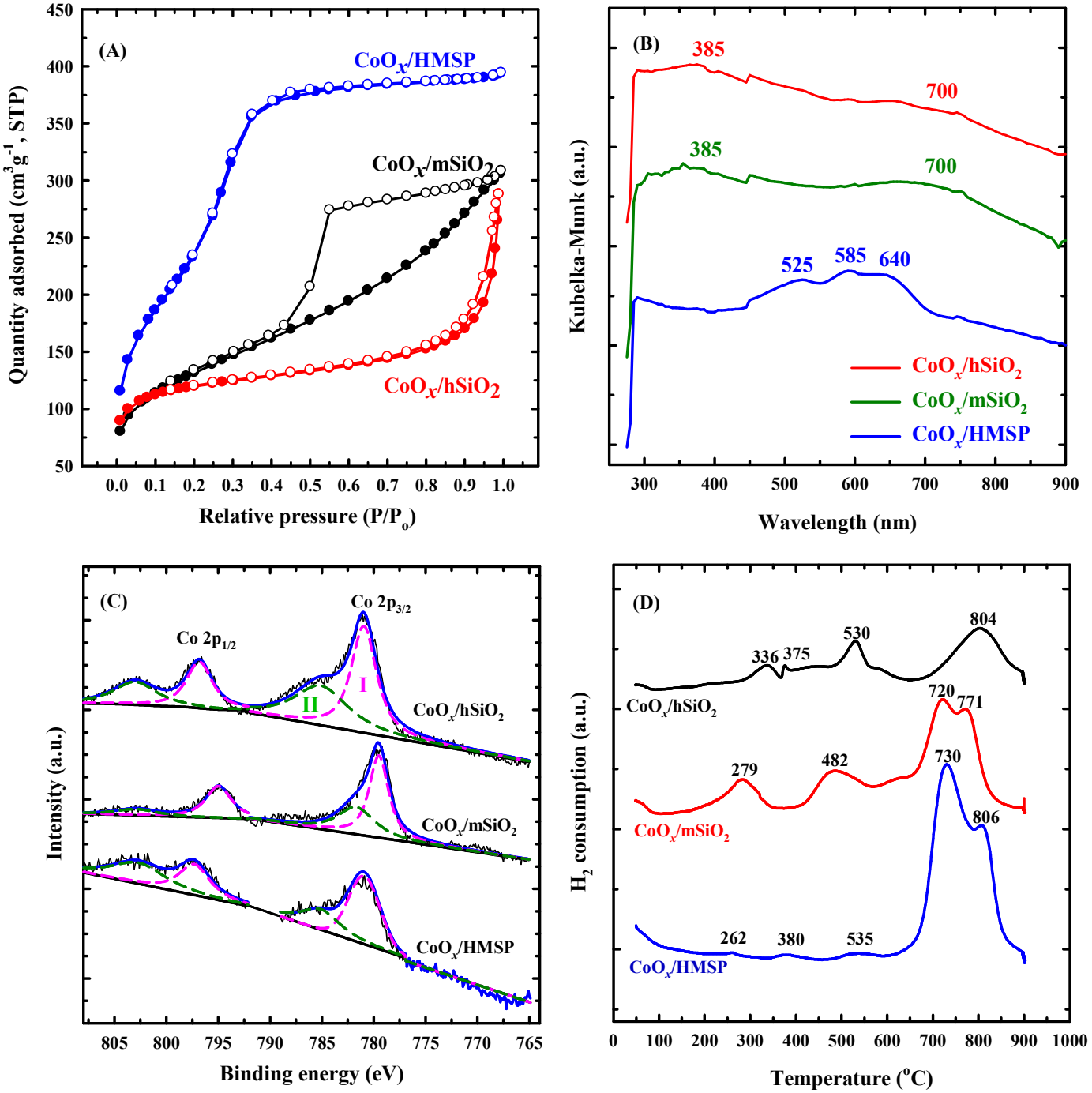

Fig. 3

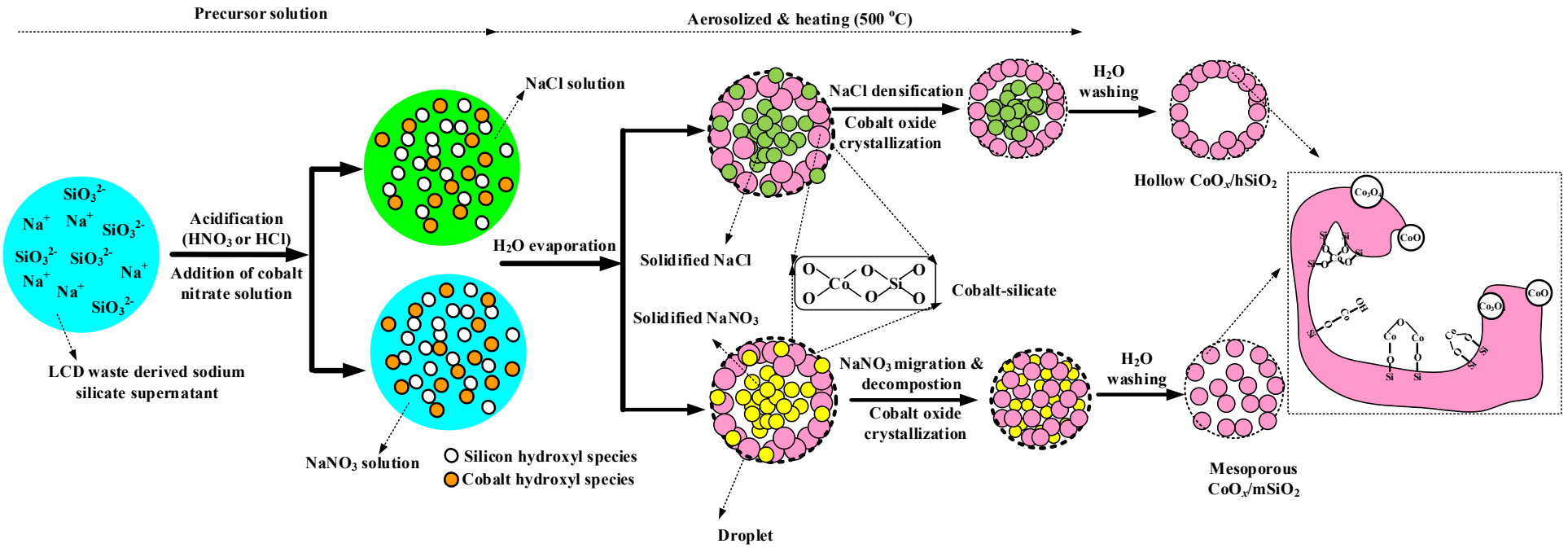

Scheme 2

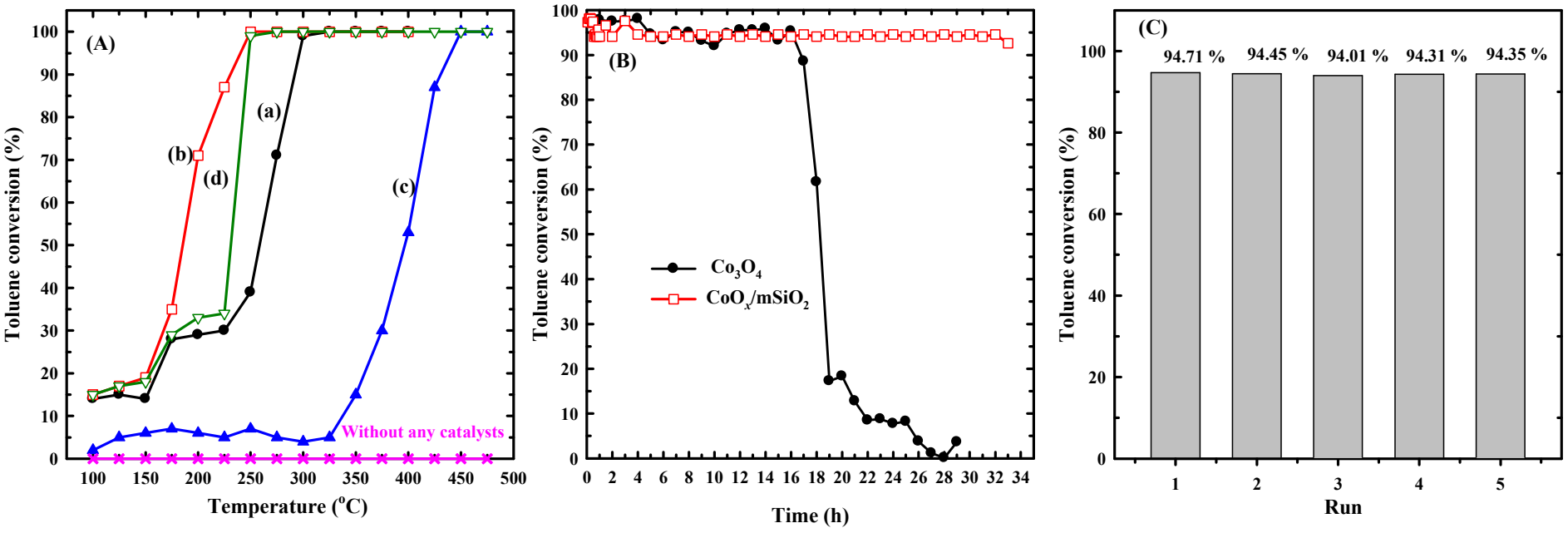

Fig. 4

View Article Online
DOI: 10.1039/C5RA27488E

Graphical abstract

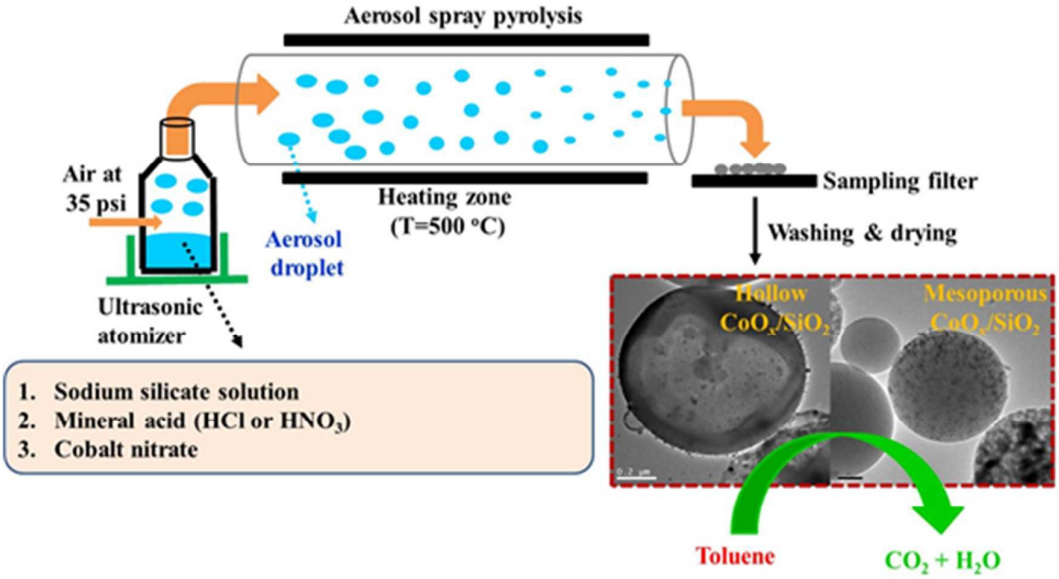

The CoO_x/SiO_2 spherical particles with hollow or mesoporous structure were successfully prepared by spray pyrolysis by using the NaCl and $NaNO_3$ as in-situ formed templates for the first time.